Egypt. J. Chem. **Vol. 67**, No. 2 pp. 513 - 526 (2024)

Egyptian Journal of Chemistry

http://ejchem.journals.ekb.eg/

Bio-sorption of Methyl blue from Synthetic wastewater onto copper\zinc oxides Bimetallic Nanoparticles Synthesized by *Fusarium oxysporum*: Equilibrium isotherms, Kinetic models, Process optimization, and Antibacterial activity

Mai Taha[1*], Ashraf Elsayed[1], Mohammed Abbas[1], Hala Fakhry [3], and Elham M Ali [2]

[1] *Botany Department, Faculty of Science, Mansoura University, Egypt*
[2] *Department of Aquatic Environmental Science, Faculty of Fish Resources, Suez University, Egypt*
[3] *City of Scientific Research and Technological Applications, (SRTA-City), New Borg El-Arab City, P.O.Box 1121934, Egypt*

Abstract

Recently, nanotechnology plays an important role in solving environmental problems such as wastewater treatment. Metal oxides such as copper oxides and zinc oxides have a role in water purification. Hence, this work aimed to remove Methyl blue dye from a synthetic wastewater sample using an environmentally friendly and cost-effective bio-sorbents; copper\ zinc oxide bimetallic (CuO\ZnO) which was synthesized by a green method using *Fussarium oxysporum* extract, and the biosorption performance was evaluated through isothermal and kinetic studies. The bio-synthesized CuO\ZnO nanoparticles were characterized by UV–Vis spectrophotometry and transmission electron microscopy (TEM). From TEM micrographs, CuO\ZnO particle size ranged from 9-40 nm and UV spectrophotometry showed the characteristic peak at 241 nm. The bio-synthesized CuO\ZnO NPs had an antibacterial activity against (*Staphylococcus aureus, Bacillus subtilis*) which represent Gram-positive bacteria, and (*Escherichia coli, Klebsiella sp*) which represent Gram-negative bacteria was studied resulting in a maximum clear zone of 1mg\mL concentration against *Escherichia coli* and *Staphylococcus aureus* more than *Klebsilla sp* and *Bacillus subtilis*. The experimental data showed that the Langmuir model and the pseudo-second-order model were fitted to the data and the biosorption capacity reached a maximum and was recorded as 68.199 mg/g.

Keywords: Antibacterial activity; methyl blue removal; *Fusarium oxysporum*; CuO\ZnO nanoparticles bio-synthesis; Equilibrium isotherms; Kinetic studies.

1. Introduction

The surface water is getting spoiled due to the release the industrial effluents which produce contaminant water of dyes, pathogens, and other pollutants in recent years [1]. It was found that the major pollutants of surface water are dyes and pigments [2]. Textile dye effluents are released into the water directly or indirectly ways which harm the environment [3]. Most dyes are toxic as a result of causing skin irritation, respiratory disease, and even the development of cancer [4, 5]. Dyes are difficult to naturally degrade due to their complex molecular structure [6-8]. There are several techniques for removing hazardous pollutants from the water e. g., precipitation [9], ion exchange separation [10], adsorption process [11], oxidation/reduction method [12], biological treatment [13], nitrifying-enriched activated sludge[14]. Among these methods, the most effective technique is adsorption due to its low cost, high selectivity, and regeneration [15, 16]. Wastewater usually contains organic dyes that are harmful to human health and the environment. Methyl blue is a cationic organic dye found in wastewater from many industries. MB is usually used in many industries such as cotton, silk, wool coloring, and other industries, It also has many medical, biological, and chemical applications [17]. MB causes health problems such as breathing difficulty, tissue necrosis, and eye burn [13, 14].

Recently a lot of bacteria have developed to be more resistant to a large number of antibiotics, making them more harmful to human health [18-21]. Antibacterial organic materials are more susceptible

*Corresponding author e-mail: maimohsentaha86@gmail.com; (Mai Taha)
Received date 26 May 2023; revised date 28 July 2023; accepted date 31 July 2023
DOI: 10.21608/ejchem.2023.213597.8029

to ambient conditions such as temperature and pressure. In the latest years, antibacterial inorganic materials have become a great ability for the control of microbes. The antibacterial activity of inorganic materials is strong even at low concentrations, especially metal oxides. The advantages of inorganic materials are their higher stability at high temperatures and pressures compared to organic materials. The most used inorganic antibacterial materials are metal nanoparticles and metal oxide nanoparticles [22-26].

Recent developments in nanotechnology and nanoscience are of great interest in many sectors such as industrial waste treatment [27-30]. Metal oxides such as copper oxides and zinc oxides have a role in water purification. Nanoparticle biosynthesis is environmentally friendly because the method does not use toxic chemicals or high energy like chemical and physical methods [31-34].The biological method was applied by using the biologically active molecules [24, 35-39] which produce from organisms like bacteria, fungi [40-43], plants, and yeasts [37, 44-49]. Fungi were preferred to bacteria due to their metal tolerance, bioaccumulation, and high ability to bind to metals. Fungi have a wide application in many fields because they produce many enzymes, are easy in the expansion process, economical feasibility, and easy handling of biomass [40, 50-53].

Bimetallic nanoparticles were produced by combining salts of two metals with the help of a reducing agent, which resulted in the production of new properties due to the synergy between the two metals [54-57]. There are different methods for bimetallic nanoparticle synthesis [58-61]. The biosynthesis of bimetallic nanoparticles is more effective because it is of high quality and non-toxic [62-64]. Bimetallic nanoparticles have been applied in wastewater treatment [65-67]. Unparalleled CuO\ZnO Bimetallic nanoparticles have shown great interest in the development of low-cost and high adsorption because of their chemical and physical properties [54, 68]. In the present project, CuO\ZnO nanoparticles were biosynthesized using the fungal extract of *Fusarium oxysporum*. Also, the antibacterial activity and the adsorption mechanism of nanoparticles were investigated.

2. Experimental

Zinc nitrate hexahydrate [Zn $(NO_3)_2.6H_2O$], and copper sulphate [$CuSO_4$] were purchased from Merck, Germany, and were used in the biosynthesis of bimetallic CuO\ZnO nanoparticles. Methyl blue [$C_{37}H_{27}N_3Na_2O_9S_3$] was also purchased from PIOCHEM and used as a contaminant dye model for evaluating the bio-sorption efficiency of nanoparticles. *Fusarium oxysporum* was collected from the mycological lab, Botany Department, Faculty of Science, Mansoura University. Pathogen bacteria strains were collected from the bacterial lab, Botany Department, Faculty of Science, Mansoura University.

2.1. Preparation of Methyl blue dye

The cationic Methyl Blue dye was used as a dye model in this study. A concentrated pure dye solution of 500 ppm was prepared in which a specific amount of dye powder was dissolved in distilled water, and different concentrations of MB (25-250 ppm) were prepared through the dilution of the as-prepared stock solution.

2.2. Biosynthesis of CuO\ZnO NPs

Fusarium oxysporum was cultured on PDA medium, and then incubated at 25°C for five days then 3-5 agar discs were inoculated in a liquid medium called MGYP media gL-1(Dextrose 10, malt extract 3, yeast extract 3, and peptone 5) for 3 days at 25 ± 2°C and 130 rpm. After the incubation period, the biomass was separated from the media by filtration, then the collected biomass was washed four times with sterile distilled water, 20 g of fresh weight biomass was transferred to 100 ml of sterile deionized water and incubated at 25 ± 2°C and 130 rpm for 24 hours. The cell-free extract was prepared by removing biomass from deionized water and adjusted to pH 6, then weight 1:1 mM of $CuSO_4$ and Zn $(NO_3)_2.6H_2O$ and added to cell-free extract and incubated at 25 ± 2°C and 130 rpm for 24 hours in dark conditions. The formed NPs were dried at 80°C calcinated at 400°C for 2 hours.

2.3. Characterization of CuO\ZnO bio-synthesized NPs

2.3.1. UV. Spectroscopy

The CuO\ZnO NPs were characterized using UV-Visible Absorption Spectroscopy using a UV-Vis spectrophotometer (JENWAY-UK) between 200 and 500 nm.

2.3.2. Transmission Electron Microscopy analysis (TEM)

Transmission Electron Microscopy analysis (TEM), Selected area electron diffraction (SAED) was investigated the crystalline structure of CuO\ZnO NPs by using HR-TEM (JEOL, JEM-2100, Tokyo, Japan).

2.3.3. X-Ray diffraction analysis (XRD)

The crystal phase NPs were identified by (XRD) measurements carried out using (D8ADVANCE, German).

2.3.4. Fourier Transform Infra-Red (FT-IR) Spectroscopy

Fourier Transform Infra-Red (FT-IR) Spectroscopy was carried out by (Bruker VERTEX 80, Germany), a combined platinum diamond ATR, comprises a diamond disk as that of an internal reflector in the range 4000-400 cm-1 with a resolution of 4 cm^{-1}, refractive index 2.4.

2.4. Antibacterial activity and MIC of CuO\ZnO NPs.

Antibacterial activity of biosynthesized NPs was investigated against pathogenic (*Staphylococcus aureus, Bacillus subtilis*) which represent Gram-positive bacteria, and (*Escherichia coli, Klebsiella sp*) which represent Gram-negative bacteria by the well-diffusion method. The tested bacteria were adjusted to a fixed bacterial number of 0.8 and spread on LB media gL-1(Sodium chloride 10, yeast extract 5, tryptone 10, and agar 20) using sterile cotton swabs [69, 70]. Wells of 9 mm diameter were made on LB agar by using a cork borer. 1 mg\mL of the prepared NPs powder was suspended in sterile deionized water and sonicated for 5 min to obtain a homogenized suspension [71, 72]. The obtained suspension was poured into each well and further incubated at 35°C ± 2 °C for 24 h. The inhibition zones (mm) were measured after incubation. For MIC determination of the myco-synthesized CuO\ZnO NPs was carried out with slight modification [44]. First, 100 µL NPs suspension from several concentrations (0.25, 0.5, 0.75, 1, 2, and 3mg/mL), 100 µL each test organism (*Escherichia coli, Bacillus subtilis, Klebsiella sp,* and *Staphylococcus aureus*) were spread on LB agar plates using sterile cotton swab the wells were made and each concentration of nanosuspension inoculated in 9 mm wells, then plates incubated at 37°C for 24h, the inhibition zone for each concentration was measured. Second, 3 mL LB broth was inoculated with 100 µL from tested bacteria, 100 µL of several NPs concentrations (1, 2, and 3mg/ml), and incubated under the conditions above. After incubation 20 µl were inoculated in LB agar media plates and incubated in the previous conditions. Results were performed by measuring the growth of the organism on agar plates.

2.5. The removal efficiency of Methyl blue dye using the bio-synthesized CuO/ZnO NPs. (Bio-sorption equilibrium isotherms and kinetic studies).

The biosynthesized CuO/ZnO NP's ability to bio-adsorb MB dye from an aqueous solution was verified by equilibrium and kinetic studies. Equilibrium bio-sorption isotherm studies and Kinetic experiments were conducted by agitating a series of flasks containing 100 mL of MB (50 ppm) solution (Kinetic studies), and (25-250ppm) (bio-sorption isotherm), respectively, and 0.1 g of the bio-synthesized CuO/ZnO NPs on Orbital mechanical shaker at an agitation speed of 150 rpm at different time intervals (5-120 min) until equilibrium was attained (Kinetic studies) and at equilibrium time (60 min) (bio-sorption isotherm). After the completion of the bio-sorption process, the bio-synthesized CuO/ZnO NPs were centrifuged at 10, 000 rpm to be able to separate them from the solution, and the residual concentration of MB was determined spectrophotometrically at 600 nm. The MB dye removal percentage (%R) and its bio-sorbed amount (q_e: at equilibrium and q_t: at time t) onto the bio-synthesized CuO/ZnO NPs were calculated using the following equations 1-3, respectively:

$$\boldsymbol{Removal\ efficiency}\ (\%) = \frac{(C_i - C_e)}{C_i} \times 100 \quad (1)$$

$$q_e = \frac{(C_i - C_e)}{m} \times V \quad (2)$$

$$q_t = \frac{(C_i - C_t)}{m} \times V \quad (3)$$

Where qt and qe (mg/g) are the amount of MB bio-sorbed per mass unit of the bio-synthesized Cu/Zn NPs at time t and at equilibrium, respectively; Ci, Ct, and Ce (mg/L) are the initial MB concentration in solution at time t and equilibrium, respectively. V (L) is the used volume of MB solution; M (g) is the used weight of the prepared bimetallic NPs.

The data of equilibrium adsorption obtained from studying the effect of initial Methyl Blue dye concentration were analyzed using the Langmuir [73] (Eq. 4) and Freundlich [74] isotherm models (Eq. 5) [75]:

$$\frac{C_e}{q_e} = \frac{1}{q_m Kl} + \frac{C_e}{q_m} \quad (4)$$

$$\ln q_e = \ln K_F + \frac{1}{n_f} \ln C_e \quad (5)$$

Where q_e is the bio-sorbed amount of Methyl Blue molecules at equilibrium (mg/g), C_e is the concentration of Methyl Blue at equilibrium (mg/L), qm is the maximum bio-sorption capacity for monolayer coverage (mg/g), K is the Langmuir constant (L/mg), and KF and nf are Freundlich constants relating to adsorption capacity and intensity, respectively.

The key parameters of the Langmuir isotherm model can be determined by the Langmuir separation factor, or an equilibrium parameter, RL, which is calculated as follows (equation 6):

$$\mathbf{RL} = \frac{1}{1 + bC0} \quad (6)$$

where C_0 is the initial MB concentration (ppm); b is Langmuir's constant; and RL indicates the type of

isotherm. If RL values between 0 and 1 indicate a favorable bio-sorption, RL > 1 indicates an unfavorable bio-sorption. Also, when RL = 0 indicates irreversible bio-sorption, RL = 1 showed a linear bio-sorption process.

The obtained data from studying the effect of contact time between Methyl Blue dye and the prepared bimetallic NPs were fitted to four common kinetic models; Pseudo-first order (PFO) (Eq. 7), pseudo-second-order (Eq. 8), Elovich (Eq. 9), and intra-particle diffusion (IPD) (Eq. 10) models that were used to predict MB adsorption kinetics onto the bio-synthesized CuO/ZnO NPs [75]. These models' corresponding equations are as follows

$$Ln(qe - qt) = \ln qe - K1t \quad (7)$$

$$\frac{t}{qt} = \frac{1}{(K2qe)2} \quad (8)$$

$$q_t = \grave{\alpha} + ß \ln t \quad (9)$$

$$qt = \frac{kidt1}{2} + c \quad (10)$$

Where q_t and q_e is the adsorbed MB amount at time t and equilibrium (mg/g) respectively. k_1 (min_1) is the first-order reaction rate constant, k_2 is the second-order reaction rate equilibrium constant (g/mg. min), is the initial adsorption rate (mg/g min), and is the extent of surface coverage and activation energy for chemisorption (g/mg), k_{id} is the intra-particle diffusion rate constant, and c give a prediction about the boundary layer thickness.

2.6. Optimization of Methyl blue removal using Central Composite Design (CCD)

Response surface methodology (RSM) was used to investigate the influence of factors like pH, contact time (min), dye concentration (ppm), and Adsorbent concentration (g\l) on the adsorption of dye on nanoparticles by CCD using four factors at five levels with five replicates at the center point to fit the data on a second order polynomial (quadratic) model.

(CCD) was utilized to optimize variable factors such as pH, contact time (min), dye concentration (ppm), and Adsorbent concentration (g\l) to achieve maximum dye removal from aqueous media by selecting the optimal conditions.

3. Results and discussion

3.1. Biosynthesis of nanoparticles by Fusarium oxysporum:

In the current study, the biosynthesis of CuO\ZnO nanoparticles using *Fusarium oxysporum* was carried out. Fig. 1 shows the growth of *Fusarium oxysporum* in MGYP media. The Bio-synthesis of CuO\ZnO NPs was observed by the color change of fungal extract from pink to pale green after the addition of copper and zinc salts and incubation for 24. Color changing due to excitation of surface plasmon after treatment with copper and zinc salts indicates the formation of CuO\ZnO NPs (Fig. 2) and the color changing is considered a preliminary confirmation of the CuO\ZnO NPs synthesis.

Fig. 1: (A) MGYP broth media, (B) MGYP broth, and *Fussarium oxysporum.*

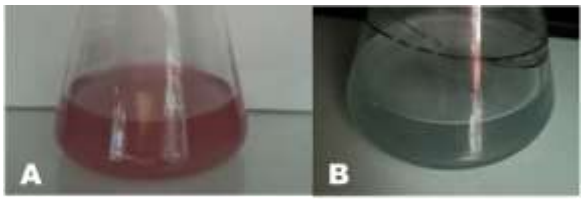

Fig. 2: (A) Cell-free extract, (B) CuO\ZnO nanoparticles.

3.2. Characterization of the bio-synthesized CuO\ZnO nanoparticle:

3.3. UV Spectroscopy:

The bio-synthesized CuO\ZnO NPs produced *by Fusarium oxysporum* were scanned by U.V-VIS spectrophotometer in a range from 200 to 500 nm. The characteristic peak of NPs was recorded at 241 nm which is indicating the presence of myco-synthesized CuO\ZnO NPs. (Fig.3)

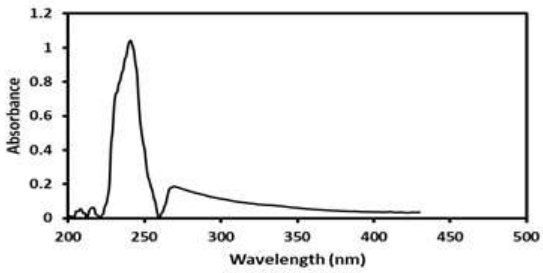

Fig. 3: U.V-VIS spectrophotometer of CuO\ZnO

3.4. X-ray Diffraction (XRD) Patterns:

The bio-synthesized CuO/ZnO NPs's crystal structure was examined using X-ray diffraction (XRD). Cu species are mostly present on ZnO in CuO-ZnO NPs, which show diffraction peaks at 32.8 (1 1 0), 52.3 (0 2 0), and 58.5 (2 0 2) [JCPDS card

no. 89-5896]. Additionally, the measured 2Θ value at 56.7 (110) demonstrates that the shape of wurtzite in ZnO has not changed [JCPDS card no. 36-1451]. The same outcomes were similar to this obtained by. The XRD pattern shows peaks attributed to the ZnO at 31.4 (1 0 0), 34.1 (0 0 2), 36.4 (1 0 1), 56.7 (1 1 0), and the peaks corresponding to the CuO at 38.009 (1 1 1), 68.9 (2 2 0) respectively. (Fig.4)

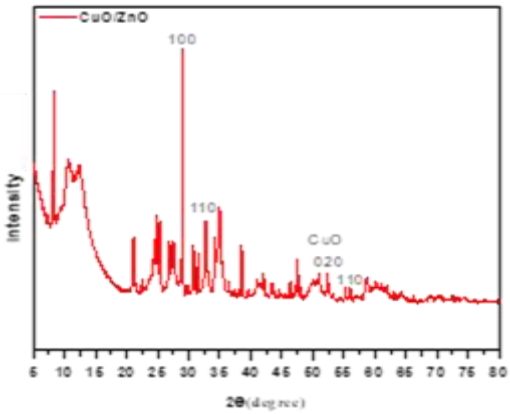

Fig. 4: XRD analysis of CuO\ZnO

3.5. Fourier Transform Infra-Red (FT-IR) Spectroscopy analysis:

Fig. 5 shows the FTIR spectra of the bio-synthesized CuO/ZnO NPs, which were obtained in the range of 500-4000 cm-1. The sample showed a characteristic peaks between (400- 509 cm^{-1}) which was correlated to the zinc oxide bond, which demonstrated the wurtzite structure of ZnO [76]. The adsorbed peak at 3336 cm-1 and 1633 cm^{-1} were attributed to O-H bending vibrations, which resulted from chemisorbed water and C=O functional group, respectively. The top at The O-H stretching mode's overtone is connected to 1423 cm^{-1}. The wavenumber of 2988 cm^{-1} is a characteristic peak of the C-H group, the presence of C=O and C-H groups was attributed to the incompletely degraded precursor of Zn to ZnO. The peaks appeared in the range of 400-700 cm^{-1} corresponding to the Cu-O bond.

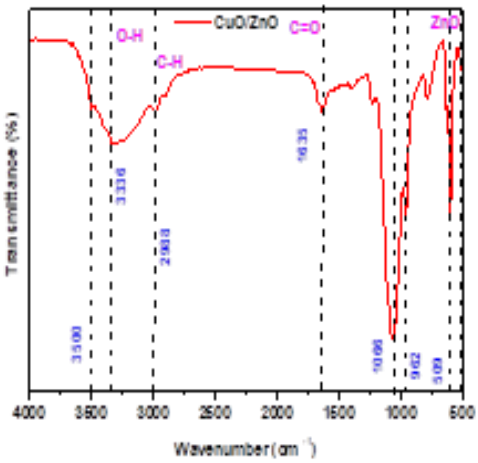

Fig. 5: FTIR spectrum of the bio-synthesized CuO\ZnO NPs.

3.6. Transmission Electron Microscope analysis (TEM)

TEM was used to determine the morphology and shape of the bio-synthesized NPs. The nanoparticles' size depends on the composition and the nature of the used medium. In this case, the nanoparticles' shape looks like a polyhedral structure, and the size distribution is wide from 9 to 40 nm. The successful biosynthesis of nano-particles is demonstrated by the TEM micrograph with spherical particles of different sizes, ranging from 9 to 40 nm. The selected area micrograph is reflecting the formation of the crystalline structure of the myco-synthesized CuO\ZnO. The variety in shape and size of CuO\ZnO NPs render to the contribution of several reducing and capping agents through biological synthesis. However, in the chemical method, it is possible to have a uniform size and shape where chemicals act as stabilizing and reducing agents [77].

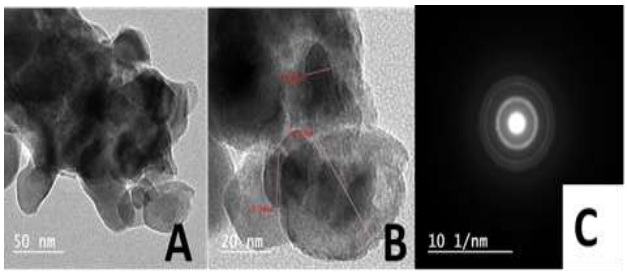

Fig. 6: (A) high magnification of TEM, (B) low magnification of TEM, (C) SAED Pattern of CuO\ ZnO nanoparticles

3.7. Antibacterial activity of bio-synthesized CuO\ZnONPs.

The antibacterial activity of the biosynthesized CuO\ZnO nanoparticles has been examined against some Gram-positive bacteria strains,(*Staphylococcus aureus and Bacillus subtilis*), and other Gram-negative bacteria strains(*Escherichia coli and Klebsilla*) (Fig. 7). The Inhibition zone (mm) of bacterial species was recorded in Table 1.Some previous studies reported that the formation of reactive oxidation species (ROS) induced the antibacterial activity of CuO\ZnO nanoparticles. ZnO and CuO NPs can produce OH and H2O2 while O2 is produced by CuO and ZnO does not. ROS can destroy cell membranes and DNA and interfere the protein function. The combination between two or more oxides nanoparticles lead to the production of ROS, which improves the antibacterial properties of NPs [78]. The bactericidal effect of CuO\ZnO nanoparticles is dependent on the concentration of nanoparticles. In present study, the initial concentration of bacteria was constant at 0.8 CFU ml-1 despite of nanoparticle concentration and microbial strain. CuO\ZnO nanoparticles have got strong antibacterial effects against all of bacteria chosen in this study. The MIC of CuO\ZnO nanoparticles were 2 mg\mL for *Bacillus subtilis*, *Staphylococcus aureus* and for *Klebsilla*, while the MIC for *Escherichia coli* was 1mg\mL for. In our results observed that CuO\ZnO NPs showed excellent bactericidal activity against a broad spectrum of bacteria. These results indicate that bio-synthesized CuO\ZnO nanoparticles are potential candidates for antibacterial agents

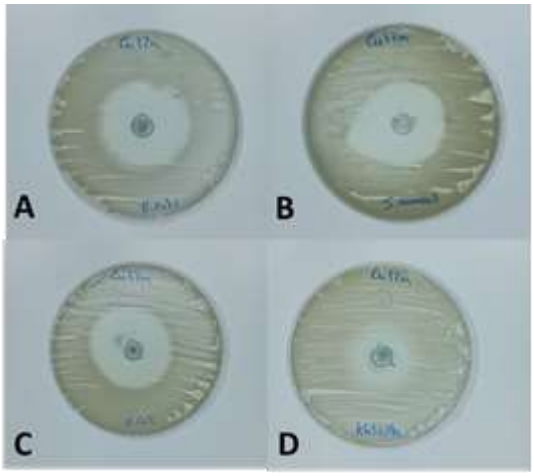

Fig. 7: (A)The inhibition zone of CuO\ZnO against *Bacillus subtilis*, (B) The inhibition zone of CuO\ZnO against *Staphylococcus aureus*, (C) The inhibition zone of CuO\ZnO against *Escherichia coli*, (D) The inhibition zone of CuO\ZnO against *Klebsilla*

Table 1: The inhibition zone values of CuO\ZnO NPs

Bacteria	Inhibition zone (mm)					
NPs (mg\mL)	0.25	0.5	0.75	1	2	3
Staphylococcus aureus	N\C	5	11	18	36	40
Escherichia coli	5	8	19	24	31	39
Bacillus subtilis	3	7	12	13	28	30
Klebsilla	N\C	N\C	15	18	25	30

Note: N\C means no inhibition zone

3.8. Bio-sorption equilibrium isotherms

The bio-sorption isotherm is usually applied to illustrate the dye molecule's distribution between liquid and solid phases at equilibrium. The experimental data were fitted to different commonly used isotherm models to find out the most suitable one for expressing it [79, 80]. The obtained isotherm data were fitted to the Langmuir and Freundlich isotherms. The applied bio-sorption isotherm models, their constants, and bio-sorption parameters were shown in Table 2 and Fig. 8. According to the obtained R2 values of the linearized plots, it was found that the Langmuir equation fitted well with the experimental data (R^2= 0.955) compared to the Freundlich equation (R^2= 0.678), suggesting a monolayer bio-sorption process, with homogeneous bio-sorption sites with similar bio-sorption capacities, as the energy of bio-sorption is constant [81]. The RL calculated values for Methyl Blue dye removal were 0.228 which lies between (0-1), meaning that the bio-sorption was favorable [82].

Unlike the Langmuir model, the Freundlich equation assumes multi-layers of bio-sorption with heterogeneous site energies. A low correlation coefficient (R^2 = 0.678) value for its linearized plot was recorded compared with the Langmuir, meaning that the description of the experimental data proves that the Langmuir isothermal model was more suitable than the Freundlich isothermal model.

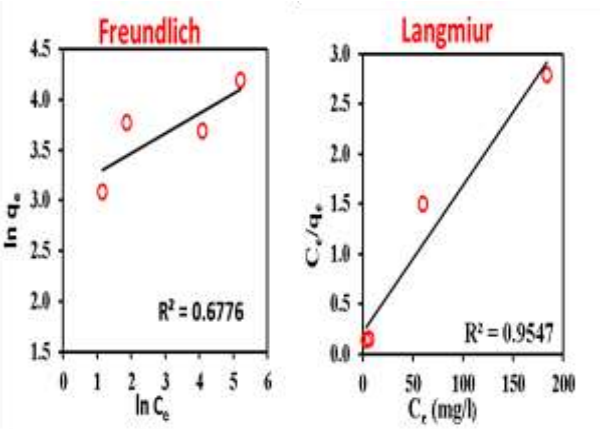

Fig. 8: Plots of Langmuir and Freundlich isotherms for the bio-sorption of Methyl Blue onto the biosynthesized CuO/ZnO NPs.

Table 2: Parameters of the applied bio-sorption isotherm models.

Isotherm parameters	The biosynthesized Cu/Zn NPs
Langmuir	
q_m (mg g^{-1}) calculated	68.199
K_L (L mg^{-1})	0.068
R^2	0.955
Freundlich	
K_F (mg1^{-} ^{1}/n L1/n g^{-1})	1185.116
nf	5.05
R^2	0.678

3.9. Bio-sorption kinetic studies

The kinetic study is relay on the removal rate of the bio-sorbate from the aqueous phase by the bio-sorbent based on the contact time between them [83]. Investigations were conducted to determine how different contact time intervals (5–120 min) between the bio-sorbent and bio-sorbate affected the bio-synthesized CuO/ZnO NPs adsorbent's ability to bio-sorb Methyl blue dye (100 ml of 50 mg/l). This factor is very important to study kinetic isotherms.

According to Fig. 9, the removal efficiency rose with contact time and reached a maximum value of 73.135%, after 60 min of contact. It was also observed that when the time was increased from 5 to 60 minutes the bio-sorption capacity (q) of the bio-synthesized NPs, was increased from 31.710 to 36.568 mg/g. This was attributed to the presence of numerous available active sites and functional groups at the bio-synthesized NPs' surface, which progressively got saturated over time, resulting in a slow dawn of the bio-sorption rate. The gained results agreed with previous studies [84, 85].

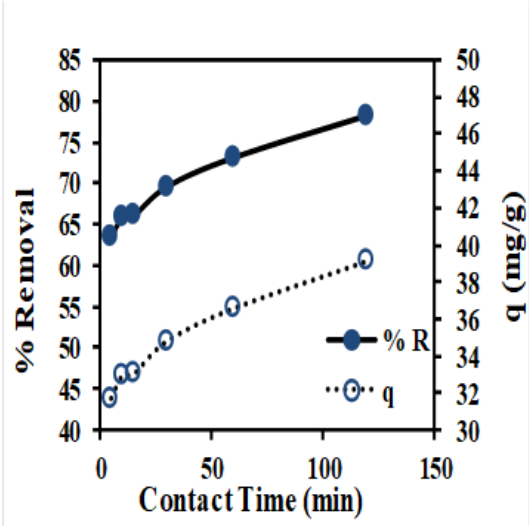

Fig. 9: Effect of Contact time (min) on the bio-sorption of Methyl Blue onto the biosynthesized CuO/ZnO NPs.

The contact time is very important in the bio-sorption process. The bio-sorption capacity of the biosynthesized CuO/ZnO NPs was evaluated at different contact times. Bio-sorption kinetics offer important information on the bio-sorption mechanisms which may be controlled by external or film diffusion, pore diffusion and bio-sorption on the pore surface, or a combination of more than one step. The kinetic models of pseudo-first order (PFO), and pseudo-second order, Elovich, and Intra-particle diffusion models were applied to the obtained experimental data to predict the bio-sorption mechanism of Methyl Blue onto the bio-synthesized NPs. The parameters of kinetic bio-sorption were illustrated in Table 4 and Fig. 9.

For the first-kinetic model, the calculated bio-sorption capacity ($q_{calculated}$) values were different from their experimental values ($q_{experimental}$), which means that this model was not good enough to describe the bio-sorption process.

The bio-sorption data is more closely suited to the PSO, based on the calculated R^2 values (0.991).consequently, the chemisorption was the rate-controlling step in the bio-sorption process, including valence forces through exchanging or sharing of electrons between bio-sorbent and bio-sorbate[60]. The calculated qe was so close to their experimental values ($q_{calculated}$= 46.953 mg/g, $q_{experimental}$= 43.519 mg/g), revealing the suitability of the PSO model to describe the data.

The simple Elovich model was applied to the obtained data, and it defines the chemisorption kinetics [86]. Table 3, illustrates that the experimental data fit well with the Elovich equation with a high R^2 value, which confirms the previous results about the chemisorption nature of the bio-sorption process using the biosynthesized NPs.

The intra-particle diffusion model was fitted to the experimental data to further explore the bio-sorption mechanism. The linearized graph in Fig. 9e and its kinetic parameters in Table 3, revealed that the biosynthesized CuO/ZnO NPs plot was divided into two stages with two straight lines that did not pass through the origin, implying that the intra-particle diffusion process was not the only rate-controlling step in the bio-sorption process [87].In the first stage, methyl blue in the aqueous phase was moved onto the NPs surface (film diffusion). While, in the second stage, the dye molecules were bio-sorbed and transferred into the pores of the NPs from their external surfaces in the second stage (intra-particle diffusion) [88]. The linearized graphs of the four kinetic models were illustrated in Fig. 10 and their kinetic parameters are in Table 3

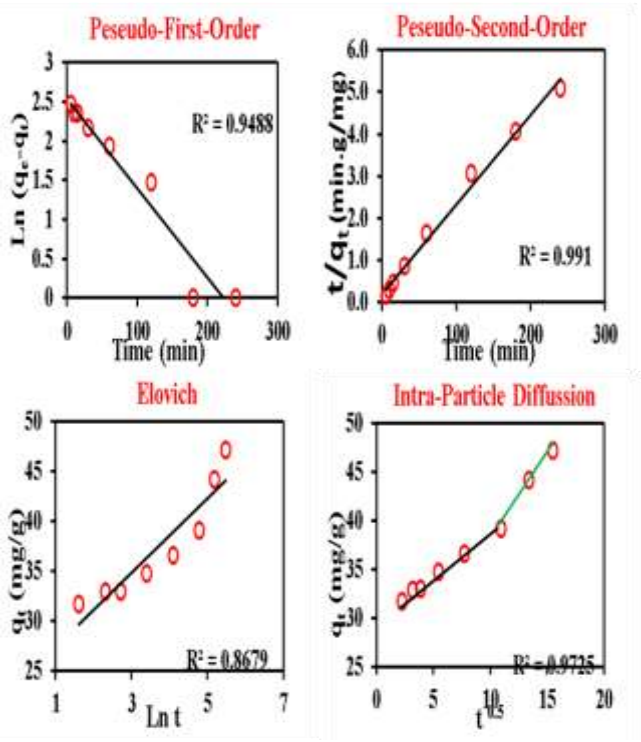

Fig. 10: different kinetic models for bio-sorption of Methyl Blue onto the biosynthesized CuO/ZnO NPs: First-order plots, Second-order plots, Elovich plots, and Intra-particle diffusion plots

Table 3: Kinetic Parameters of different kinetic models for bio-sorption of Methyl Blue onto the biosynthesized CuO/ZnO NPs

Kinetic Model		The biosynthesized CuO/ZnO) NPs
Pseudo-First-Order	q_e(mg/g) Calculated	12.605
	q_e (mg/g) Experimental	43.519
	k_1(min^{-1})	-0.01
	R^2	0.949
Pseudo-Second-Order	q_e (mg/g) Calculated	46.953
	q_e (mg/g) Experimental	43.519
	k_2(g/mg min)	0.002
	R^2	0.991
Elovich	β (g/mg)	3.699
	α (mg/g min)	23.752
	R^2	0.868
Intra-particle Diffusion	ki_d,	1.116
	I	28.727
	R^2	0.973

3.10. Optimization of Methyl blue removal using Central Composite Design (CCD)

Central composite design (CCD) was used as the most traditional method. It was used to study the individual and combined factors effects on the responses. The CCD helps avoid unnecessary experimentation and helps explore synergies between factors. A total of 27 runs for four factors of MB concentration, CuO\ZnO dosage, pH, and contact time were designed. The response was measured by measuring the MB removal percent.

Predictions from the fitted linear model versus actual experimental values. The line represents perfect predictions and the distance represents residual aberrations. Predictions for higher response values have fewer residuals and are therefore much better than low values that have more deviations from the line (Figure 11).

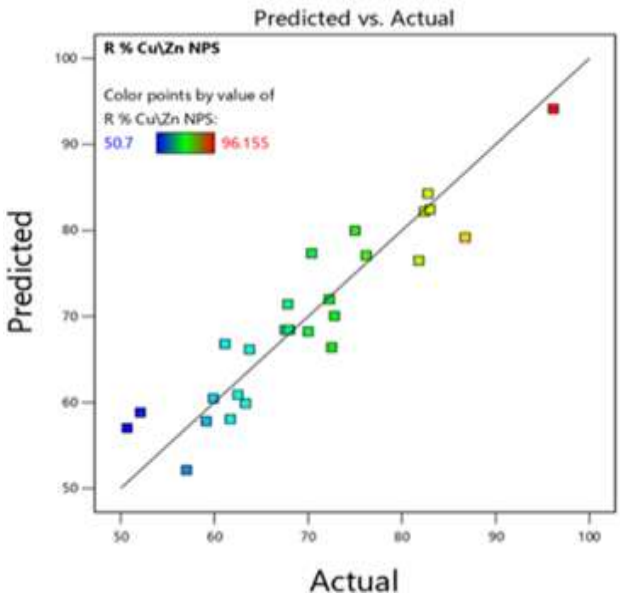

Fig. 11: The predicted response values versus the actual response values for MB removal using CuO\ZnO NPs

Fitted model prediction vs residual error (difference from actual experimental values) shown in Figure 12. The residual value is normalized by the standard deviation (sigma) of the residues for each model. This provides a visual diagnosis of the model's external predictions. Perfect predictions do not have any residual errors, and points close to the zero line represent better predictions.

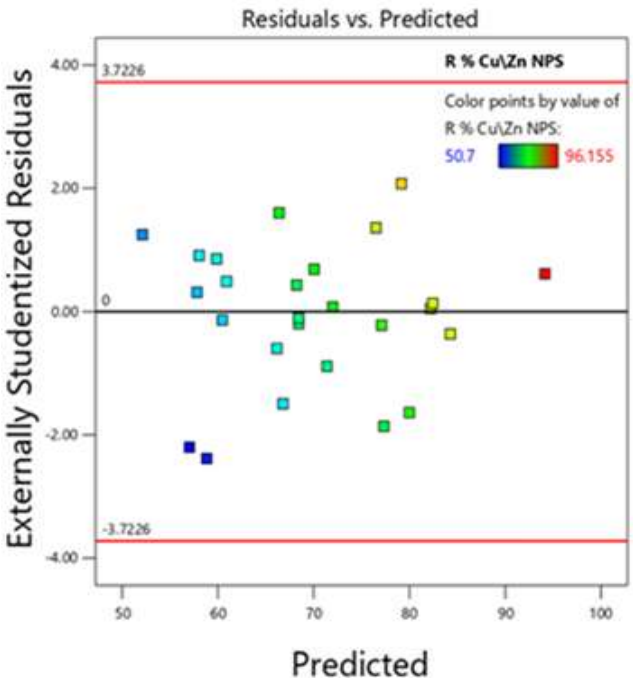

Fig. 12: Predicted vs. normal residual errors plots of MB removal using CuO\ZnO NPs

Model selection was performed using backward feature selection based on a p-value threshold close to the α=0.1 level. Starting with a quadratic model that includes all the linear and interaction terms the model is refined iteratively by removing the least significant term and refitting until no terms are above the desired threshold. The final selected model is in the table 4 which is a reduced quadratic model.

Table 4. ANOVA for Reduced Quadratic model (R % CuO\ZnO NPs).

Source	Sum of Squares	df	Mean Square	F-value	p-value
Model	2652.84	9	294.76	12.34	< 0.0001
A-Dye Conc	15.74	1	15.74	0.6587	0.4282
B-Adsorbent Conc	95.67	1	95.67	4.00	0.0616
C-pH	1870.42	1	1870.42	78.29	< 0.0001
D-Contact time	22.40	1	22.40	0.9376	0.3465
AC	180.86	1	180.86	7.57	0.0136
BD	56.79	1	56.79	2.38	0.1416
B^2	85.66	1	85.66	3.59	0.0754
C^2	97.57	1	97.57	4.08	0.0593
D^2	134.46	1	134.46	5.63	0.0297
Residual	406.17	17	23.89		
Lack of Fit	406.05	15	27.07	444.98	0.0022
Pure Error	0.1217	2	0.0608		
Cor Total	3059.01	26			

Fit Statistics

Std. Dev.	4.89	**R^2**	0.8672
Mean	69.80	**Adjusted R^2**	0.7969
C.V. %	7.00	**Adeq Precision**	14.1288

Final Model Equation

R % Cu\Zn NPS =
+68.44 -0.8098***A** +2.00***B** +8.83***C** +0.9661***D**
+3.36***AC** -1.88***BD** +1.89***B²** +2.02***C²** -2.37***D²**

The residual table (Table 5) contained the predictions obtained using the fitted model equation above for each data point and comparing it to the actual experimental values by taking the difference between them to get the residual (error) for the model.

Table 5. Residual Table for **(R % CuO\ZnO NPs).**

Run Order	Actual Value	Predicted Value	Residual	Standard Order
1	82.40	82.21	0.1959	14
2	72.25	72.00	0.2503	19
3	59.90	60.47	-0.5685	1
4	63.74	66.17	-2.43	9
5	67.95	68.44	-0.4857	27
6	82.99	82.43	0.5597	16
7	59.13	57.83	1.30	10

8	50.70	57.04	-6.34	23
9	61.71	58.05	3.65	12
10	67.84	71.40	-3.57	5
11	61.14	66.82	-5.67	18
12	62.50	60.90	1.60	24
13	81.81	76.51	5.31	6
14	82.78	84.27	-1.48	8
15	96.16	94.16	2.00	22
16	67.55	68.44	-0.8857	25
17	72.80	70.06	2.74	17
18	76.19	77.10	-0.9096	13
19	70.00	68.23	1.77	3
20	57.04	52.13	4.91	2
21	75.00	79.99	-4.99	20
22	52.11	58.84	-6.73	21
23	72.52	66.40	6.13	11
24	70.37	77.33	-6.96	15
25	86.76	79.16	7.59	7
26	68.00	68.44	-0.4357	26
27	63.33	59.89	3.44	4

The response surface is maximized with respect to the CuO\ZnO absorption response using a Hill Climbing algorithm and interaction graphs for the response surface is produced by varying the two factors in the graph and fixing the other two at optimal levels (Fig. 13).

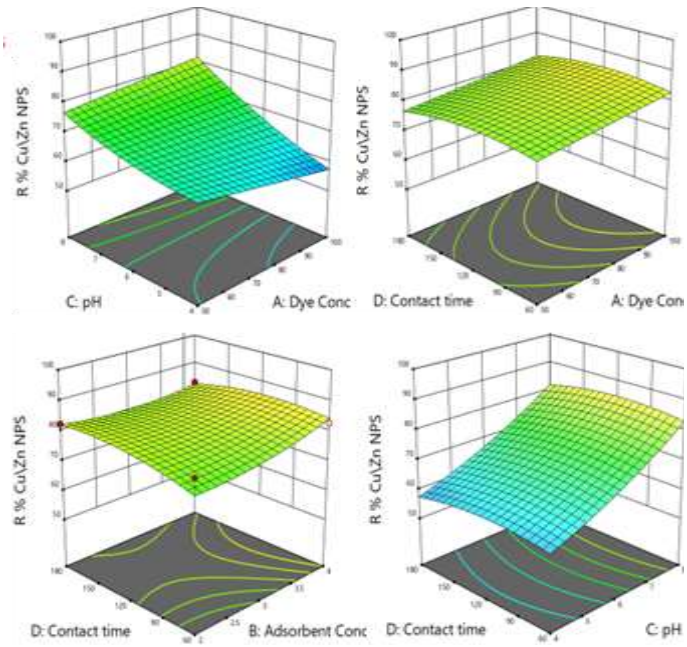

Fig. 13: 3D Surface plots of MB removal using CuO\ZnO NPs

The optimized conditions for the factors such as MB concentration, CuO\ZnO dosage, pH and contact time were found to be 75 ppm, 3 g\L, 10 and 120 min, respectively. In these conditions, the removal percentage for MB was 96.155%.

4. Conclusion

In the present study, the extract of *Fusarium oxysporum* has successfully mediated the synthesis of CuO \ ZnO nanoparticles due to containing polysaccharides, enzymes, and other compounds which act as stabilizing and reducing agents. XRD analysis showed the crystalline structure and the purity of CuO\ZnO NPs, which revealed the diffraction patterns for NPs. TEM analysis confirmed that the shape and particle sizes of the CuO\ZnO NPs were found in the nano-scale range. The antibacterial activity and adsorption property studies of CuO\ZnO were carried out.

5. Refrences

1. Bhuiyan, M.S.H., M.Y. Miah, S.C. Paul, T.D. Aka, O. Saha, M.M. Rahaman, M.J.I. Sharif, O. Habiba, and M. Ashaduzzaman, Green synthesis of iron oxide nanoparticle using *Carica papaya* leaf extract: application for photocatalytic degradation of remazol yellow RR dye and antibacterial activity. Heliyon, 2020. **6**(8): p. e04603.
2. Sahu, N., S. Rawat, J. Singh, R.R. Karri, S. Lee, J.-S. Choi, and J.R. Koduru, Process optimization and modeling of methylene blue adsorption using zero-valent iron nanoparticles synthesized from sweet lime pulp. Applied Sciences, 2019. **9**(23): p. 5112.
3. Lachheb, H., E. Puzenat, A. Houas, M. Ksibi, E. Elaloui, C. Guillard, and J.-M. Herrmann, Photocatalytic degradation of various types of dyes in water by UV-irradiated titania. Applied Catalysis B: Environmental, 2002. **39**: p. 75-90.
4. Immich, A.P.S., A.A.U. de Souza, and S.M.d.A.G. Ulson, Removal of Remazol Blue RR dye from aqueous solutions with Neem leaves and evaluation of their acute toxicity with Daphnia magna. Journal of Hazardous Materials, 2009. **164**(2-3): p. 1580-1585.
5. Khan, S. and A. Malik, Environmental and health effects of textile industry wastewater, in Environmental deterioration and human health. 2014, Springer. p. 55-71.
6. Fan, Y., H.-J. Liu, Y. Zhang, and Y. Chen, Adsorption of anionic MO or cationic MB from MO/MB mixture using polyacrylonitrile fiber hydrothermally treated with hyperbranched polyethylenimine. Journal of Hazardous Materials, 2015. **283**: p. 321-328.
7. Wang, Y., A. López-Valdivieso, T. Zhang, T. Mwamulima, X. Zhang, S. Song, and C. Peng, Preparation of microscale zero-valent iron-fly ash-bentonite composite and evaluation of its adsorption performance of crystal violet and methylene blue dyes. Environmental Science Pollution Research, 2017. **24**(24): p. 20050-20062.

8. Zhu, N., T. Yan, J. Qiao, and H. Cao, Adsorption of arsenic, phosphorus and chromium by bismuth impregnated biochar: Adsorption mechanism and depleted adsorbent utilization. Chemosphere, 2016. **164**: p. 32-40.
9. Rasalingam, S., R. Peng, and R.T. Koodali, An insight into the adsorption and photocatalytic degradation of rhodamine B in periodic mesoporous materials. Applied Catalysis B: Environmental, 2015. **174**: p. 49-59.
10. Alkan, M., M. Doğan, Y. Turhan, Ö. Demirbaş, and P. Turan, Adsorption kinetics and mechanism of maxilon blue 5G dye on sepiolite from aqueous solutions. Chemical Engineering Journal, 2008. **139**(2): p. 213-223.
11. Doğan, M., Y. Özdemir, and M. Alkan, Adsorption kinetics and mechanism of cationic methyl violet and methylene blue dyes onto sepiolite. Dyes Pigments, 2007. **75**(3): p. 701-713.
12. Mall, I.D., V.C. Srivastava, and N.K. Agarwal, Removal of Orange-G and Methyl Violet dyes by adsorption onto bagasse fly ash—kinetic study and equilibrium isotherm analyses. Dyes pigments, 2006. **69**(3): p. 210-223.
13. Zhang, P., I. Lo, D. O'Connor, S. Pehkonen, H. Cheng, and D. Hou, High efficiency removal of methylene blue using SDS surface-modified ZnFe2O4 nanoparticles. Journal of colloid interface science, 2017. **508**: p. 39-48.
14. Zirak, M., A. Abdollahiyan, B. Eftekhari-Sis, and M. Saraei, Carboxymethyl cellulose coated Fe3O4@ SiO2 core–shell magnetic nanoparticles for methylene blue removal: equilibrium, kinetic, and thermodynamic studies. Cellulose, 2018. **25**(1): p. 503-515.
15. Annadurai, G., L.Y. Ling, and J.-F. Lee, Adsorption of reactive dye from an aqueous solution by chitosan: isotherm, kinetic and thermodynamic analysis. Journal of hazardous materials, 2008. **152**(1): p. 337-346.
16. Rauf, M., S. Bukallah, F. Hamour, and A. Nasir, Adsorption of dyes from aqueous solutions onto sand and their kinetic behavior. Chemical Engineering Journal, 2008. **137**(2): p. 238-243.
17. Mardani, H.R., M. Forouzani, M. Ziari, and P. Biparva, Visible light photo-degradation of methylene blue over Fe or Cu promoted ZnO nanoparticles. Spectrochimica Acta Part A: Molecular Biomolecular Spectroscopy, 2015. **141**: p. 27-33.
18. Alsamhary, K.I., Eco-friendly synthesis of silver nanoparticles by *Bacillus subtilis* and their antibacterial activity. Saudi Journal of Biological Sciences, 2020. **27**(8): p. 2185-2191.
19. Li, X., Y. Cong, M. Ovais, M.B. Cardoso, S. Hameed, R. Chen, M. Chen, and L. Wang, Copper-based nanoparticles against microbial infections. Wiley Interdisciplinary Reviews: Nanomedicine Nanobiotechnology, 2023: p. e1888.
20. Sánchez-López, E., D. Gomes, G. Esteruelas, L. Bonilla, A.L. Lopez-Machado, R. Galindo, A. Cano, M. Espina, M. Ettcheto, and A. Camins, Metal-based nanoparticles as antimicrobial agents: an overview. Nanomaterials, 2020. **10**(2): p. 292.
21. Munir, M.U., A. Ahmed, M. Usman, and S. Salman, Recent advances in nanotechnology-aided materials in combating microbial resistance and functioning as antibiotics substitutes. International Journal of Nanomedicine, 2020: p. 7329-7358.
22. Thi, T.U.D., T.T. Nguyen, Y.D. Thi, K.H.T. Thi, B.T. Phan, and K.N. Pham, Green synthesis of ZnO nanoparticles using orange fruit peel extract for antibacterial activities. RSC advances, 2020. **10**(40): p. 23899-23907.
23. Lallo da Silva, B., M.P. Abuçafy, E. Berbel Manaia, J.A. Oshiro Junior, B.G. Chiari-Andréo, R.C.R. Pietro, and L.A. Chiavacci, Relationship between structure and antimicrobial activity of zinc oxide nanoparticles: An overview. International journal of nanomedicine, 2019: p. 9395-9410.
24. Mohd Yusof, H., R. Mohamad, U.H. Zaidan, and N.A. Abdul Rahman, Microbial synthesis of zinc oxide nanoparticles and their potential application as an antimicrobial agent and a feed supplement in animal industry: a review. Journal of animal science biotechnology, 2019. **10**: p. 1-22.
25. Gharpure, S., A. Akash, and B. Ankamwar, A review on antimicrobial properties of metal nanoparticles. Journal of nanoscience nanotechnology, 2020. **20**(6): p. 3303-3339.
26. Bezza, F.A., S.M. Tichapondwa, and E.M. Chirwa, Fabrication of monodispersed copper oxide nanoparticles with potential application as antimicrobial agents. Scientific Reports, 2020. **10**(1): p. 16680.
27. Gangadoo, S., D. Stanley, R.J. Hughes, R.J. Moore, and J. Chapman, The synthesis and characterisation of highly stable and reproducible selenium nanoparticles. Inorganic Nano-Metal Chemistry, 2017. **47**(11): p. 1568-1576.
28. Naseem, T. and T. Durrani, The role of some important metal oxide nanoparticles for wastewater and antibacterial applications: A review. Environmental Chemistry Ecotoxicology, 2021. **3**: p. 59-75.
29. Rambabu, K., G. Bharath, F. Banat, and P.L. Show, Green synthesis of zinc oxide nanoparticles using Phoenix dactylifera waste as bioreductant for effective dye degradation and antibacterial performance in wastewater treatment. Journal of hazardous materials, 2021. **402**: p. 123560.
30. Al-Rawashdeh, N.A., O. Allabadi, and M.T. Aljarrah, Photocatalytic activity of graphene oxide/zinc oxide nanocomposites with embedded

metal nanoparticles for the degradation of organic dyes. ACS omega, 2020. **5**(43): p. 28046-28055.
31. Tyagi, P.K., D. Gola, S. Tyagi, A.K. Mishra, A. Kumar, N. Chauhan, A. Ahuja, and S. Sirohi, Synthesis of zinc oxide nanoparticles and its conjugation with antibiotic: Antibacterial and morphological characterization. Environmental Nanotechnology, Monitoring Management, 2020. **14**: p. 100391.
32. Carrapiço, A., M.R. Martins, A.T. Caldeira, J. Mirão, and L. Dias, Biosynthesis of Metal and Metal Oxide Nanoparticles Using Microbial Cultures: Mechanisms, Antimicrobial Activity and Applications to Cultural Heritage. Microorganisms, 2023. **11**(2): p. 378.
33. de Jesus, R.A., G.C. de Assis, R.J. de Oliveira, J.A.S. Costa, C.M.P. da Silva, M. Bilal, H.M. Iqbal, L.F.R. Ferreira, and R.T. Figueiredo, Environmental remediation potentialities of metal and metal oxide nanoparticles: mechanistic biosynthesis, influencing factors, and application standpoint. Environmental Technology Innovation, 2021. **24**: p. 101851.
34. Jeevanandam, J., S.F. Kiew, S. Boakye-Ansah, S.Y. Lau, A. Barhoum, M.K. Danquah, and J. Rodrigues, Green approaches for the synthesis of metal and metal oxide nanoparticles using microbial and plant extracts. Nanoscale, 2022. **14**(7): p. 2534-2571.
35. Zhao, X., S. Zhang, C. Li, B. Zheng, and H. Gu, Application of zinc oxide nanopowder for two-dimensional micro-gas sensor array. Journal of Materials Synthesis Processing, 1997. **5**: p. 227.
36. Mittal, S. and A. Roy, Fungus and plant-mediated synthesis of metallic nanoparticles and their application in degradation of dyes, in Photocatalytic degradation of dyes. 2021, Elsevier. p. 287-308.
37. Abomuti, M.A., E.Y. Danish, A. Firoz, N. Hasan, and M.A. Malik, Green synthesis of zinc oxide nanoparticles using *salvia officinalis* leaf extract and their photocatalytic and antifungal activities. Biology, 2021. **10**(11): p. 1075.
38. Thiruvengadam, M., I.-M. Chung, T. Gomathi, M.A. Ansari, V. Gopiesh Khanna, V. Babu, and G. Rajakumar, Synthesis, characterization and pharmacological potential of green synthesized copper nanoparticles. Bioprocess biosystems engineering, 2019. **42**: p. 1769-1777.
39. Pavithran, S., M. Pappuswamy, Y. Annadurai, V.A. Armugam, and T. Periyaswamy, Green Synthesis of Copper Nanoparticles, Characterization and Their Applications. Journal of Applied Life Sciences International, 2020. **23**(7): p. 10-24.
40. Elsayed, A., G.M. El-Shamy, and A.A. Attia, Biosynthesis, Characterization, and Assessment of Zirconia Nanoparticles by *Fusarium oxysporum* species as Potential Novel Antimicrobial and Cytotoxic Agents. Egyptian Journal of Botany, 2022. **62**(2): p. 507-522.
41. Elsayed, A., K. Hashish, and A.-D.J.J.o.E.S. Sherief, Production and characterization OF silver nanoparticles synthesized BY nanoparticles synthesized BY *FUSARIUM oxysporum FUSARIUM oxysporum*. 2015. **44**(4): p. 681-691.
42. Santos, T.S., T.M. Silva, J.C. Cardoso, R.L.d. Albuquerque-Júnior, A. Zielinska, E.B. Souto, P. Severino, and M.d.C. Mendonça, Biosynthesis of silver nanoparticles mediated by entomopathogenic fungi: Antimicrobial resistance, nanopesticides, and toxicity. Antibiotics, 2021. **10**(7): p. 852.
43. Qu, Y., X. Li, S. Lian, C. Dai, Z. Jv, B. Zhao, and H. Zhou, Biosynthesis of gold nanoparticles using fungus *Trichoderma* sp. WL-Go and their catalysis in degradation of aromatic pollutants. IET nanobiotechnology, 2019. **13**(1): p. 12-17.
44. Soliman, H., A. Elsayed, and A. Dyaa, Antimicrobial activity of silver nanoparticles biosynthesised by *Rhodotorula* sp. strain ATL72. Egyptian Journal of Basic Applied Sciences, 2018. **5**(3): p. 228-233.
45. Saleh, H., A. Abdelrazak, A. Elsayed, H. El-Shishtawy, and Y. Osman, Correction to: Optimizing production of a biopesticide protectant by black yeast. Egyptian Journal of Biological Pest Control, 2022. **32**(1): p. 1-1.
46. Mali, S.C., A. Dhaka, C.K. Githala, and R. Trivedi, Green synthesis of copper nanoparticles using *Celastrus paniculatus* Willd. leaf extract and their photocatalytic and antifungal properties. Biotechnology Reports, 2020. **27**: p. e00518.
47. Nieto-Maldonado, A., S. Bustos-Guadarrama, H. Espinoza-Gomez, L.Z. Flores-López, K. Ramirez-Acosta, G. Alonso-Nuñez, and R.D. Cadena-Nava, Green synthesis of copper nanoparticles using different plant extracts and their antibacterial activity. Journal of Environmental Chemical Engineering, 2022. **10**(2): p. 107130.
48. Amer, M. and A. Awwad, Green synthesis of copper nanoparticles by Citrus limon fruits extract, characterization and antibacterial activity. Chemistry International, 2020. **7**(1): p. 1-8.
49. Demissie, M.G., F.K. Sabir, G.D. Edossa, and B.A. Gonfa, Synthesis of zinc oxide nanoparticles using leaf extract of *lippia adoensis* (koseret) and evaluation of its antibacterial activity. Journal of Chemistry, 2020. **2020**: p. 1-9.
50. Kalpana, V., B.A.S. Kataru, N. Sravani, T. Vigneshwari, A. Panneerselvam, and V.D. Rajeswari, Biosynthesis of zinc oxide nanoparticles using culture filtrates of *Aspergillus niger*: Antimicrobial textiles and dye degradation studies. OpenNano, 2018. **3**: p. 48-55.

51. Shamim, A., T. Mahmood, and M.B. Abid, Biogenic synthesis of zinc oxide (ZnO) nanoparticles using a fungus (*Aspargillus niger*) and Their Characterization. International Journal of Chemistry, 2019. **11**(2): p. 119.
52. Abdelhakim, H., E. El-Sayed, and F. Rashidi, Biosynthesis of zinc oxide nanoparticles with antimicrobial, anticancer, antioxidant and photocatalytic activities by the endophytic *Alternaria tenuissima*. Journal of Applied Microbiology, 2020. **128**(6): p. 1634-1646.
53. Saitawadekar, A. and U.B. Kakde, Green synthesis of copper nanoparticles using *Aspergillus flavus*. J. Crit. Rev, 2020. **7**(9).
54. Rosbero, T.M.S. and D.H. Camacho, Green preparation and characterization of tentacle-like silver/copper nanoparticles for catalytic degradation of toxic chlorpyrifos in water. Journal of environmental chemical engineering, 2017. **5**(3): p. 2524-2532.
55. Ameen, F., Optimization of the synthesis of fungus-mediated bi-metallic Ag-Cu nanoparticles. Applied Sciences, 2022. **12**(3): p. 1384.
56. Kamal, A., M. Saba, A. Kamal, M. Batool, M. Asif, A.M. Al-Mohaimeed, D.A. Al Farraj, D. Habib, and S. Ahmad, Bioinspired Green Synthesis of Bimetallic Iron and Zinc Oxide Nanoparticles Using Mushroom Extract and Use against *Aspergillus niger*; The Most Devastating Fungi of the Green World. Catalysts, 2023. **13**(2): p. 400.
57. Kumaravel, J., K. Lalitha, M. Arunthirumeni, and M.S. Shivakumar, Mycosynthesis of bimetallic zinc oxide and titanium dioxide nanoparticles for control of Spodoptera frugiperda. Pesticide Biochemistry Physiology, 2021. **178**: p. 104910.
58. Zaleska-Medynska, A., M. Marchelek, M. Diak, and E. Grabowska, Noble metal-based bimetallic nanoparticles: the effect of the structure on the optical, catalytic and photocatalytic properties. Advances in colloid interface science, 2016. **229**: p. 80-107.
59. Berta, L., N.-A. Coman, A. Rusu, and C. Tanase, A review on plant-mediated synthesis of bimetallic nanoparticles, characterisation and their biological applications. Materials, 2021. **14**(24): p. 7677.
60. Sasireka, K.S. and P. Lalitha, Biogenic synthesis of bimetallic nanoparticles and their applications. Reviews in Inorganic Chemistry, 2021. **41**(4): p. 223-244.
61. Idris, D.S. and A. Roy, Synthesis of Bimetallic Nanoparticles and Applications—An Updated Review. Crystals, 2023. **13**(4): p. 637.
62. Mittal, A.K., Y. Chisti, and U.C. Banerjee, Synthesis of metallic nanoparticles using plant extracts. Biotechnology advances, 2013. **31**(2): p. 346-356.
63. López-Ubaldo, F., V. Sánchez-Mendieta, O.F. Olea-Mejía, S.G.-P. María, and R.A.M. Luckie, Biosynthesis of Ag/Cu bimetallic nanoparticles using *Ricinus communis* and their antibacterial and antifungical activity. Advances in Natural Sciences: Nanoscience Nanotechnology, 2020. **11**(2): p. 025018.
64. Tiri, R.N.E., F. Gulbagca, A. Aygun, A. Cherif, and F. Sen, Biosynthesis of Ag–Pt bimetallic nanoparticles using *propolis* extract: Antibacterial effects and catalytic activity on NaBH4 hydrolysis. Environmental Research, 2022. **206**: p. 112622.
65. Al-Haddad, J., F. Alzaabi, P. Pal, K. Rambabu, and F. Banat, Green synthesis of bimetallic copper–silver nanoparticles and their application in catalytic and antibacterial activities. Clean Technologies Environmental Policy, 2020. **22**: p. 269-277.
66. Scaria, J., P. Nidheesh, and M.S. Kumar, Synthesis and applications of various bimetallic nanomaterials in water and wastewater treatment. Journal of environmental management, 2020. **259**: p. 110011.
67. Dlamini, N.G., A.K. Basson, and V.S.R. Pullabhotla, Synthesis and Characterization of Various Bimetallic Nanoparticles and Their Application. Applied Nano, 2023. **4**(1): p. 1-24.
68. Verma, A., S. Pal, P. Verma, V. Srivastava, R. Mandal, and I. Sinha, Ag-Cu bimetallic nanocatalysts for p-nitrophenol reduction using a green hydrogen source. Journal of environmental chemical engineering, 2017. **5**(6): p. 6148-6155.
69. Li, W.-R., X.-B. Xie, Q.-S. Shi, H.-Y. Zeng, Y.-S. Ou-Yang, and Y.-B. Chen, Antibacterial activity and mechanism of silver nanoparticles on Escherichia coli. Applied microbiology biotechnology, 2010. **85**(4): p. 1115-1122.
70. Tiri, R.N.E., F. Gulbagca, A. Aygun, A. Cherif, and F. Sen, Biosynthesis of Ag–Pt bimetallic nanoparticles using *propolis* extract: Antibacterial effects and catalytic activity on NaBH4 hydrolysis. Environmental Research, 2022. **206**: p. 112622.
71. Morones, J.R., J.L. Elechiguerra, A. Camacho, K. Holt, J.B. Kouri, J.T. Ramírez, and M.J. Yacaman, The bactericidal effect of silver nanoparticles. Nanotechnology, 2005. **16**(10): p. 2346.
72. Padilla-Cruz, A., J. Garza-Cervantes, X. Vasto-Anzaldo, G. García-Rivas, A. León-Buitimea, and J. Morones-Ramírez, Synthesis and design of Ag–Fe bimetallic nanoparticles as antimicrobial synergistic combination therapies against clinically relevant pathogens. Scientific Reports, 2021. **11**(1): p. 1-10.
73. Langmuir, I., The adsorption of gases on plane surfaces of glass, mica and platinum. Journal of the American Chemical society, 1918. **40**(9): p. 1361-1403.
74. Freundlich, H., Über die adsorption in lösungen. Zeitschrift für physikalische Chemie, 1907. **57**(1): p. 385-470.

75. Fakhry, H., M. El-Sonbati, B. Omar, R. El-Henawy, Y. Zhang, and E.-K. Marwa, Novel fabricated low-cost hybrid polyacrylonitrile/polyvinylpyrrolidone coated polyurethane foam (PAN/PVP@ PUF) membrane for the decolorization of cationic and anionic dyes. Journal of Environmental Management, 2022. **315**: p. 115128.
76. Habibi, M.H., B.J.J.o.I. Karimi, and E. Chemistry, Preparation of nanostructure CuO/ZnO mixed oxide by sol–gel thermal decomposition of a CuCO3 and ZnCO3: TG, DTG, XRD, FESEM and DRS investigations. 2014. **20**(3): p. 925-929.
77. Ahluwalia, V., J. Kumar, R. Sisodia, N.A. Shakil, and S. Walia, Green synthesis of silver nanoparticles by *Trichoderma harzianum* and their bio-efficacy evaluation against Staphylococcus aureus and Klebsiella pneumonia. Industrial Crops Products, 2014. **55**: p. 202-206.
78. Asamoah, R., A. Yaya, B. Mensah, P. Nbalayim, V. Apalangya, Y. Bensah, L. Damoah, B. Agyei-Tuffour, D. Dodoo-Arhin, and E. Annan, Synthesis and characterization of zinc and copper oxide nanoparticles and their antibacteria activity. Results in Materials, 2020. **7**: p. 100099.
79. El-Kady, M., M. El-Aassar, O.A. El Batrawy, M.S. Ibrahim, H.S. Hassan, and H. Fakhry, Equilibrium and Kinetic Behaviors of Cationic Dye Decolorization Using Poly (AN-co-Py)/ZrO_2 Novel Nanopolymeric Composites. Advances in Polymer Technology, 2018. **37**(3): p. 740-752.
80. Yildirim, A., Kinetic, equilibrium and thermodynamic investigations for the bio-sorption of dyes onto crosslinked *Pleurotus ostreatus*-based bio-composite. International Journal of Environmental Analytical Chemistry, 2020. **102**(17): p. 1-16.
81. Ahmad, I., M.A. Jamal, M. Iftikhar, A. Ahmad, S. Hussain, H. Asghar, M. Saeed, A.B. Yousaf, R.R. Karri, and N.S. Al-kadhi, Lanthanum-zinc binary oxide nanocomposite with promising heterogeneous catalysis performance for the active conversion of 4-nitrophenol into 4-aminophenol. Coatings, 2021. **11**(5): p. 537.
82. Ho, Y., J. Porter, and G. McKay, Equilibrium isotherm studies for the sorption of divalent metal ions onto peat: copper, nickel and lead single component systems. Water, air, soil pollution, 2002. **141**(1): p. 1-33.
83. Milani, P.A., J.L. Consonni, G. Labuto, and E.N.V.M. Carrilho, Agricultural solid waste for sorption of metal ions, part II: competitive assessment in multielemental solution and lake water. Environmental Science Pollution Research, 2018. **25**(36): p. 35906-35914.
84. El-Aassar, M., H. Fakhry, A.A. Elzain, H. Farouk, and E.E. Hafez, Rhizofiltration system consists of chitosan and natural *Arundo donax* L. for removal of basic red dye. International journal of biological macromolecules, 2018. **120**: p. 1508-1514.
85. Gagliano, E., M. Sgroi, P.P. Falciglia, F.G. Vagliasindi, and P. Roccaro, Removal of poly-and perfluoroalkyl substances (PFAS) from water by adsorption: Role of PFAS chain length, effect of organic matter and challenges in adsorbent regeneration. Water research, 2020. **171**: p. 115381.
86. El-Amier, Y.A., A. Elsayed, M.A. El-Esawi, A. Noureldeen, H. Darwish, and H. Fakhry, Optimizing the biosorption behavior of Ludwigia stolonifera in the removal of lead and chromium metal ions from synthetic wastewater. Sustainability, 2021. **13**(11): p. 6390.
87. Ma, X., C. Liu, D.P. Anderson, and P.R. Chang, Porous cellulose spheres: Preparation, modification and adsorption properties. Chemosphere, 2016. **165**: p. 399-408.
88. Tran, H.N., S.-J. You, A. Hosseini-Bandegharaei, and H.-P. Chao, Mistakes and inconsistencies regarding adsorption of contaminants from aqueous solutions: a critical review. Water research, 2017. **120**: p. 88-116.